# Fault Compartmentalization in a Mature Clastic Reservoir: An Example from Elk Hills Field, California*

**Alan P. Morris[1], Kevin Smart[2], David A. Ferrill[2], Nathaniel Reish[3], and Peter F. Cowell[3]**

Search and Discovery Article #40907 (2012)
Posted March 31, 2012

*Adapted from extended abstract prepared in conjunction with oral presentation at AAPG Annual Convention and Exhibition, Long Beach, California, April 22-25, 2012


[1]Southwest Research Institute, San Antonio, TX, United States (amorris@swri.org)
[2]Southwest Research Institute, San Antonio, TX, United States
[3]Occidental of Elk Hills, Bakersfield, CA, United States

## Abstract

Mature and aging clastic-dominated hydrocarbon fields commonly become increasingly difficult to produce, causing lower economic return than initially forecast. A major cause of this reduced economic viability is compartmentalization, defined as limitation on the ability to produce hydrocarbons resulting from permeability barriers within a field. Three primary causes of compartmentalization are (i) structural variations in permeability, (ii) stratigraphic variations in permeability, and (iii) permeability reduction resulting from compaction adjacent to producing wellbores. Recognition and delineation of compartmentalization permits formulation of development and depletion plans to maximize recovery and economic value. Here we examine one of several reservoir-scale faults that compartmentalize a portion of the Eastern Shallow Oil Zone, Elk Hills Field, California. Using well log, stratigraphic, structural, and pressure data, we apply standard fault seal analyses to the selected fault. Results are compared with known pressure conditions across the fault, and show the fault capable of supporting pressure differentials two to three times those expected from standard fault seal measures. Reasons for this apparently anomalous behavior include (i) reduction of pore fluid pressure resulting from hydrocarbon production over the last 90 years has reduced the slip tendency of all faults in the field, and concomitantly increased their sealing potential; (ii) fault zones contain structures that may not seal the fault over millions of years, but create permeability barriers at production time scales; and (iii) the presence of uninterpreted small-displacement faults adjacent to mapped faults that contribute to permeability reduction - important at production, but not trap formation, time scales.

## Fault Seal Behavior

A major cause of reduced economic viability of aging hydrocarbon fields is compartmentalization by faults (Smalley and Muggeridge, 2010; Fox and Bowman, 2010). Reservoir compartmentalization by fault seal is common in faulted porous sandstones (Van Hulten, 2010). There are three principal components of fault seal behavior (Smith, 1980; Yielding et al., 2010). First is the lithological juxtaposition across a fault, for example sand on sand juxtaposition is less likely to seal than sand on shale (Smith, 1980; Allan, 1989; Corona et al., 2008; Van Hulten,

2010). Second, are deformation products within and adjacent to the fault. For example, remnants of the host lithologies are frequently smeared into a fault zone, and these may reduce the transmissibility of the fault. Clay-rich lithologies are likely to reduce fault zone permeability more than clay-poor lithologies, and this premise forms the basis for estimating fault seal potential using approaches such as calculating shale gouge ratio (SGR) and clay smear potential (Yielding et al., 1997 and references therein). Faults are typically zones with finite thickness within which displacement has been localized, and the thickness and internal structure of a fault zone affect its transmissibility. In addition to the fault zone itself, faults with displacements greater than a few meters usually have a damage zone that extends into both the footwall and hanging wall of the fault (Ferrill et al., 2011), so that changes in permeability associated with the fault are likely to be transitional through this damage zone. Third, is the stress state on discontinuities within the fault zone. Fault and fracture surfaces experiencing high slip tendency (ratio of resolved shear to normal stress on a surface) are more likely to be transmissive than those experiencing low slip tendency (Barton, et al., 1995; Heffer et al., 1995; Morris et al., 1996; Zoback et al., 1996; Ferrill et al., 1999; Fox and Bowman, 2010), and therefore changing stress states can affect the sealing behavior of a fault.

Despite the complexity of estimating fault sealing characteristics, in the realm of reservoir modeling fault seal analysis is often reduced to estimating a single transmissibility value for a fault zone (Manzocchi et al., 1999, 2010), which introduces the further uncertainty of estimating fault zone thickness. Fault seal analysis is essentially the estimation of fault transmissibility based on the assumed effects of three factors (juxtaposition, fault zone material, and stress) on the intrinsic permeability of the fault zone, and an assumed fault zone thickness.

## Static Versus Dynamic Seals

In the case of reservoir compartmentalization by faults, there are two categories of fault seal (Jolley et al., 2010), commonly referred to as (i) static seals, those that have sufficiently low transmissibility to be effective seals over geological time scales, and (ii) dynamic seals, those that are seals or baffles to flow at production time scales. Static seals form the basis on which many prospects depend, and few would worry about such a seal becoming tighter during production. Dynamic seals, however, are only fully revealed during production, and may be dynamic not just in respect to the flow of fluid, but their intrinsic permeability and/or transmissibility may also be time-dependent. A fault with low intrinsic permeability may have existed within the reservoir for the lifetime of the trap, but its low transmissibility has not been an impediment to equilibration of pressures and compositions over the long geological time periods during which the trap evolved. Such a fault will only be revealed as a compartment boundary if production activities generate a cross-fault pressure difference that cannot equilibrate over production time scales, i.e., weeks to months to years. This would be a dynamic seal, but the intrinsic properties of the fault remain unchanged from pre- to syn-production times. However, if, during production, a fault experiences a reduction in transmissibility either as a result of changing fluid interaction or changes in intrinsic permeability, such a fault would have a changing transmissibility character over the production lifetime of the field.

## Juxtaposition and Shale Gouge Ratio

Of the three factors that affect fault seal, juxtaposition and fault zone clay or shale content are the most commonly studied and applied to fault seal analysis (Manzocchi et al., 2010). A typical workflow would take the Allan juxtaposition diagram of a fault and attempt to

populate it with values of a property that somehow represent the fluid-flow characteristics of the fault at every point on its surface. The most commonly used fault property is some representation of the clay or shale content of the fault zone, and most popular among these is SGR (Yielding et al., 2002, and references therein). Although a generally positive correlation is reported between SGR and across-fault pressure differential (Yielding, 2002), widespread use of SGR as a proxy for intrinsic fault zone permeability has led to the recognition that there is no simple and universal relationship between such measures and permeability. Calibration of these methods is required, and the more local the calibration, the better the relationship (Yielding et al., 2010). Implicit in this approach is the assumption that clay or shale content in the fault zone is the primary determinant of a fault zone's intrinsic permeability. The calibration methodology, because of this a priori assumption, is bound to find a relationship between clay/shale content and fault seal behavior. Stress, although occasionally analyzed (Bolås and Hermanrud, 2002; Wiprut and Zoback, 2002) is usually treated as a leak threat where stress conditions approach those likely to generate fault reactivation (critical stress), and is not viewed from the reverse perspective that departure from a critical stress state may increase the sealing potential of a fault.

## A Different Scenario

Consider a reservoir prior to production containing intra-reservoir faults, experiencing uniform pressure and fluid characteristics and elevated pore-fluid pressures (Figure 1). If initial production decreases the pore-fluid pressure and drives the ambient stress state away from the critical reactivation stress state for faults in the reservoir, this may result in a reduction of the intrinsic permeability of faults, thereby causing compartmentalization. The resultant search for fault properties that provide a history match to production data results in a set of intrinsic fault rock permeabilities that are much lower than those actually measured from core, a not uncommon finding (Fisher and Jolley, 2007), because, in our scenario, the fault permeability is being controlled by the stress state experienced by the fault zone and not by its clay content.

## Geologic Background Case Study

Elk Hills Field lies near the southern end of the San Joaquin Valley, California, approximately 30 miles (48 km) WSW of Bakersfield, and just west of the axis of the Great Valley Syncline (Reid, 1995; Figure 2). Elk Hills is one of a series of fold-thrust structures east of the Temblor Range, which is bounded on the west by the San Andreas Fault (Nicholson, 1990). The Eastern Shallow Oil Zone (ESOZ) is developed over one of these anticlines and consists primarily of sands and shales of the early Pliocene (~ 3 to 4 Ma) Etchegoin Formation. Although these structures are fundamentally contractional, the predominant mode of faulting over the crest of the Elk Hills structure at the level of the ESOZ is extensional (Maher et al., 1975). The overall geometry of these faults indicates extension oblique to the principal anticline axis. We interpret this extensional deformation to be the result of outer-arc bending directed across and along the anticlinal axis as the anticline grew and propagated along strike (Ratliff, 1992). Some of these faults extend to the ground surface and the fundamental fold has been active from Miocene time to the present (Maher et al., 1975; Graham et al., 1999).

We analyze one of fifty-two faults within the ESOZ that seal over production time scales and compartmentalize the field. We use well log, stratigraphic, structural, and pressure data from this faulted reservoir and apply standard fault seal analysis to a specific fault, and then compare these results with the known pressure conditions across the fault.

The official Elk Hills discovery well, Standard Oil Company's "Hay No. 1", was drilled in 1919. As part of the Naval Petroleum Reserve, the field experienced limited production until the oil embargo of the 1970's, when in 1976 the field was opened to commercial production. During this early production phase, faulting in the ESOZ was not considered to have had an appreciable effect on the trapping of oil (Maher et al., 1975). Occidental Petroleum purchased the property and took over operation of the field in 1998. Occidental acquired a 3-D seismic survey over the field immediately after purchase, and completed an extensive integrated reservoir characterization of the ESOZ that details the complex stratigraphy and faulting. This improved geologic interpretation facilitated design of a development and depletion program to maximize recovery from this compartmentalized, gravity drainage dominated reservoir.

Average fluid pressures encountered in the crest of the ESOZ during initial drilling were approximately 1500 psi (10.27 MPa). Pressures had dropped to 850 psi (5.82 MPa) by 1941, and since then have declined to about 100 – 200 psi (0.68 – 1.37 MPa). Pressure depletion as a result of oil and gas production from the ESOZ has led to gravity-driven, down-structure flow of the remaining oil becoming the dominant drainage mechanism. The current production method is pressure-maintenance of the secondary gas cap via gas injection. Gravity drainage has highlighted the ability of faults to compartmentalize the reservoir, creating oil "bands" as draining fluid is dammed up and diverted by these faults. Recognition of this compartmentalization has led to the development of an effective production strategy whereby the up-dip sides of faults are targets for production-well drilling. In this study we analyzed the sealing potential of one of the faults in terms of juxtaposition relationships, shale gouge ratio, fault rock, and stress state in an attempt to understand the transmissibility of the fault zone.

## Stratigraphy

Two major sand reservoirs in the ESOZ are the Etchegoin Sub-Scalez 1 (SS1) and the Etchegoin Upper Sub- Scalez 2 (USS2; Figure 3). These sands are interpreted to have been deposited in a tide-dominated estuarine system (Maher et al., 1975; Reid, 1995). The locally used distinction between sand and clay (or shale) is 35 % clay ($V_{clay} = 0.35$). $V_{clay}$ is based on core analysis and the ESOZ petrophysical model tied to core. Stratigraphic thicknesses and $V_{clay}$ values were obtained from fourteen wells with complete logged sections through the SS1 and USS2 intervals and for at least 150 ft (46 m) above the top of the SS1. Thirteen of the fourteen wells are within 500 ft (152 m) of the fault analyzed in the study and all are within 1000 ft (305 m).

## Fault Seal Analysis – Faulting and Bed Juxtaposition

Faults mapped that cut the ESOZ reservoir sands, based on 3-D seismic data, detailed well-log correlations, and identification of missing section in a 3500-well dataset, have NE-SW strikes (Figure 2), 50 – 60° dips, and approximately half of the faults dip to the NW and half to the SE. Throw (vertical component of displacement) varies from 5 ft (1.5 m; the limit of resolution) to 400 ft (122 m). Fault FB11C-12SE (located between wells 44NE-10G and 52XSE-1G) consists of multiple segments, and was chosen for this analysis because of the

availability of well log data, formation pressure measurements, and high level of confidence in the fault interpretation (Figure 2). At the level of the SS1 and USS2 horizons this fault has a strike of 060 – 070°, dips to the SSE at approximately 55°, and has a throw of 20 – 150 ft (6 – 46 m) averaging ~60 ft (18 m). Depth to the reservoir intervals of interest is approximately 3000 ft (914 m).

Fault displacements were calculated from fault polygon data extracted from a 3-D geologic model of the field for the appropriate stratigraphic horizons. The geologic model was constructed using all available seismic and well data. Fault polygons were also used to construct cutoff diagrams against fault FB11C-12SE for the tops and bases of the SS1 and USS2 reservoir units.

Subject to local thickness variations, the SS1 sand is juxtaposed with itself across the fault wherever the throw is less than about 100 ft (30 m). The USS2 is rarely self-juxtaposed within the area of detailed study, except where throw is less than 40 ft (12 m). There is, however, a large area of juxtaposition of SS1 reservoir sand (in the hanging wall) with USS2 reservoir sand (in the footwall; Figure 4).

## Fault Seal Analysis – Pressure Differential

Repeat formation test (RFT) pressure data from more than twenty wells adjacent to the fault were compiled for the juxtaposed USS2 in the footwall and SS1 in the hanging wall of fault FB11C-12SE (Figure 4). USS2 (footwall) has fluid pressures of 430 – 500 psi (2.9 – 3.4 MPa) in the study area, whereas SS1 (hanging wall) has fluid pressures of 200 psi (1.4 MPa). This fault sustains a pressure differential of 230 to 300 psi (1.6 to 2.1 MPa) at the production timescale.

## Fault Seal Analysis – Shale Gouge Ratio

Shale gouge ratios for the detailed study area of fault FB11C-12SE were calculated at 0.5 ft (0.15 m) vertical intervals for each of fourteen wells using the stratigraphic sections and log data extracted from each well chosen for the study, and fault throw values obtained from the 3-D geologic model. The vertical strings of calculated SGR values from each of the fourteen wells were projected onto the fault and contoured to provide a continuous map of shale gouge ratio (Figure 5). Values of SGR vary from near zero to almost 60%; however, more than half of the fault area has SGR less than 30%. The area of lowest SGR (lowest sealing potential) coincides with an area of continuous sand-on-sand juxtaposition across the fault, constituting high risk of leakage.

## Fault Seal Analysis – Fault Zone Structure

Core samples of fault FB11C-12SE at the stratigraphic level of interest are not available. Most core sampling is intended to provide permeability and porosity data for the complete reservoir section and coring jobs are specifically planned to avoid faulted sections where reservoir intervals will be missing. Production wells are drilled to avoid penetrating faults within the reservoir interval to maximize wellbore exposure to productive reservoir. However, faults with displacements undetectable by seismic data, and less than can be inferred from well interpretations, are present in core samples. One such fault (stratigraphic throw ≈ 2 ft (0.61 m)) cuts the top of the SS1 in well 37NE-27S (Figure 6).

Deeper in the same well a series of faults with unknown displacements (but probably less than 1 ft (0.3 m)) cut the base of SS1. Core from well 61X-2G contains a fault with a displacement of 0.08 ft (0.03 m) that cuts the top of SS1 (Figure 7). Although these faults have small displacements, their internal structure provides insights into the nature of larger faults and indicates the widespread occurrence of small-displacement (subseismic) faults.

Fault zones are characterized by fine-grained material formed by both grain size reduction and entrainment of material into the fault (Figure 6 and Figure 7). Fault zones typically consist of several fault segments that together create barriers or baffles to fluid flow that, although discontinuous, impart a tortuosity to flow pathways across the fault zone. Cross-fault permeability is further reduced by the occurrence of synthetically dipping layers (layers dipping in the same direction as the fault; Figure 7).

## Juxtaposition, SGR, and Pressure Differential

The area of juxtaposition of the SS1 and USS2 reservoirs along most of the fault section in this study coincides with an area of low (< 30%) SGR (Figure 4 and Figure 5). For the current depth of burial (approximately 3000 ft [914 m]) this portion of the fault should be capable of supporting long term, or static, pressure differentials of no more than ~70 psi (0.5 MPa; Yielding, 2002). However, short term, dynamic, pressure differentials in excess of 200
psi (1.4 MPa) are measured (Figure 8).

## Discussion

The pressure and fault seal analysis data for fault FB11C-12SE could be used to define a calibration point for dynamic sealing of faults in the Elk Hills Field. The pressure differential being supported by the fault is between 230 and 300 psi (1.6 to 2.1 MPa), the range of shale gouge ratios within the area of juxtaposition between upper SS1 in the hanging wall and USS2 in the footwall is 10 to 40% (Figure 5). The physical significance of this is that the intrinsic permeability and resultant transmissibility of the fault zone with these SGR values are low enough that at production time scales pressure differentials of between 230 and 300 psi (1.6 to 2.1 MPa) will not equilibrate.

Another means by which the fault's transmissibility could be reduced is the presence of a sufficiently wide damage zone containing permeability-reducing structures such as sub-seismic faults, grain size reduction, and synthetically dipping (to small faults) sedimentary layering (Figure 6 and Figure 7). Such features would have been present prior to production, but would not necessarily have been revealed as potential barriers to flow if the fault's transmissibility had been high enough to permit pressure equilibration over geological time scales.

SGR, sub-seismic faults, and other permeability-reducing features of the fault zone are essentially fixed through the lifetime of the field. However, it is possible that the sealing capacity of the fault has evolved through the development period of Elk Hills Field. One of the most significant changes over the 100 years of production has been the decrease in pore fluid pressure as inferred from fluid pressures measured in the crest of the structure, and which have declined from approximately 1500 psi (10.27 MPa) at discovery to the present-day 100 – 200 psi

(0.68 – 1.37 MPa). Faults and fractures experiencing a state of stress close to the critical stress for reactivation are likely to have high intrinsic permeability (Barton, et al., 1995; Heffer et al., 1995; Morris et al., 1996; Zoback et al., 1996; Ferrill et al., 1999; Fox and Bowman, 2010). Townend and Zoback (2000) show that the tendency for a fault to be hydraulically conductive depends on the ratio of shear to normal stress, or slip tendency (Morris et al., 1996), acting on the fault, and that a slip tendency of approximately 0.6 or above is most conducive to fluid flow. We take the reverse of this observation to suggest that faults and fractures experiencing stress states that are not near to the critical reactivation state are likely to have low intrinsic permeability.

The maximum depth of burial of the faulted rocks in the ESOZ at Elk Hills was approximately 3000 ft (914 m). Average overburden density was approximately 1700 kg/m3. Triaxial test data from well 63-3G provided sufficient information (compressive strength of about 3000 psi [20.75 MPa] at a confining pressure of 1200 psi [8.25 MPa]) to infer a range of Hoek-Brown failure envelopes that would represent rocks of the ESOZ reservoirs at Elk Hills (Hoek and Brown, 1988). We assume that the fluid pressure during faulting was close to the initial fluid pressure recorded in the ESOZ reservoirs at Elk Hills during discovery drilling. Based on the fact that the faulting is related to amplification of the underlying fold, which has been active in the last 2 to 3 million years and may still be growing (Maher et al., 1975), we further infer that the stress state was close to failure conditions prior to discovery of the field. Decreasing fluid pressure resulting from hydrocarbon production has caused the stress state at Elk Hills to evolve away from a critical stress state. Thus faults that might have been in a state of critical stress, and therefore leaky, prior to discovery, may no longer leak because their slip tendency has decreased concomitantly with fluid pressure (Figure 9).

## Conclusions

Across-fault juxtaposition and shale gouge ratio analyses fail to identify the fault in this investigation as a sealing or compartmentalizing fault. Using this as a basis for local calibration of the SGR method for dynamic seals assumes that SGR is the permeability-controlling variable. We propose consideration of the production stress history as a possible alternative for providing insight into the sealing behavior of the fault, and others like it. One of the most significant measurable changes in the field since production began is the average fluid pressure. One consequence of the decrease in pore fluid pressure will have been the evolution of stress states acting on faults away from critical stress and leaky conditions to more stable and less leaky conditions. In the case of Elk Hills Field, reservoir compartmentalization has been recognized and exploited by an effective production strategy. In other situations, for example offshore, conditions may not be as fortuitous and close monitoring of fluid pressures and fault seal behavior might provide an early warning concerning developing compartmentalization.

## References

Allan, U.S., 1989, Model for hydrocarbon migration and entrapment within faulted structures: AAPG Bulletin, v. 73, p. 803–811.

Barton, C.A., M.D. Zoback, and D. Moos, 1995, Fluid flow along potentially active faults in crystalline rock: Geology, v. 23, p. 683–686.

Bolås, H.M.N., and C. Hermanrud, 2002, Rock stress in sedimentary basins – implications for trap integrity: *in* A.G. Koestler, and R. Hunsdale, (eds.), Hydrocarbon Seal Quantification. NPF Special Publication 11, p. 17–35.

Bowman, M., 2008, Tackling the challenges and minimizing the impacts of compartmentalization on reservoir performance, *in* Reservoir Compartmentalization: The Geological Society of London Petroleum Group Meeting, 5-6 March 2008, p. 8.

Corona, F.V., J.S. Davis, S.J. Hippler, and P.J. Vrolijk, 2008, Multi-fault analysis scorecard: Success of stochastic approach in fault seal prediction, *in* Reservoir Compartmentalization: The Geological Society of London Petroleum Group Meeting, 5-6 March 2008, p. 46.

Ferrill, D.A., A.P. Morris, R.N. McGinnis, K.J. Smart, and W.C. Ward, 2011, Fault zone deformation and displacement partitioning in mechanically layered carbonates: The Hidden Valley Fault, central Texas: AAPG Bulletin, v. 95, p. 1383–1397.

Ferrill, D.A., J. Winterle, G. Wittmeyer, D. Sims, S. Colton, A. Armstrong, and A.P. Morris, 1999, Stressed rock strains groundwater at Yucca Mountain, Nevada: GSA Today, v. 9/5, p. 1–8.

Fisher, Q.J., and S.J. Jolley, 2007, Treatment of faults in production simulation models, *in* S.J. Jolley, D. Barr, J.J. Walsh, and R.J. Knipe, (eds.), Structurally Complex Reservoirs, Geological Society of London Special Publications 292, p. 219–233.

Fox, R.J., and M.B.J. Bowman, 2010, The challenges and impact of compartmentalization in reservoir appraisal and development: Geological Society London Special Publications, v. 347, p. 9–23.

Graham, S.E., T.M. Mahony, J.L. Blissenbach, J.J. Mariant, C.M. Wentworth, and T.W. Dibblee, 1999, Regional geologic map of San Andreas and related faults in Carrizo Plain, Temblor, Caliente and La Panza Ranges and vicinity, California: A digital database: U.S. Geological Survey Open-File Report 99-14.

Harris, S.D., R.J. Knipe, S. Freeman, Z. Khatir, A. Brown, R.K. Davies, and A. Li, 2008, The influence of fault geometric and property uncertainty modeling on reservoir compartmentalization, *in* Reservoir Compartmentalization: The Geological Society of London Petroleum Group Meeting, 5-6 March 2008, p. 66.

Heffer, K.J., R.J. Fox, and C.A. McGill, 1995, Novel techniques show links between reservoir flow directionality, earth stress, fault structure, and geomechanical changes in mature waterfloods: Society of Petroleum Engineers, SPE Paper 30711, p. 91-98.

Hoek, E., and E.T. Brown, 1988, The Hoek-Brown failure criterion - a 1988 update: Proc. 15th Canadian Rock Mech. Symp, J.C. Curran, (ed.), Toronto, Dept. Civil Engineering, University of Toronto, p. 31-38

Jolley, S.J., Q.J. Fisher, and R.B. Ainsworth, 2010, Reservoir compartmentalization: an introduction: Geological Society London Special Publications 2010, v. 347, p. 1-8.

Maher, J.C., R.D. Carter, and R.J. Lantz, 1975, Petroleum Geology of Naval Petroleum Reserve No. 1, Elk Hills, Kern County, California: United States Geological Survey Professional Paper 912, p. 109

Manzocchi, T., J.J. Walsh, P. Nell, and G. Yielding, 1999, Fault transmissibility multipliers for flow simulation models: Petroleum Geoscience, v. 5, p. 53-63.

Manzocchi, T., C. Childs, and J.J. Walsh, 2010, Faults and fault properties in hydrocarbon flow models: Geofluids, v. 10, p. 94-113.

Morris, A.P., D.A. Ferrill, and D.B. Henderson, 1996, Slip tendency and fault reactivation: Geology, v. 24, p. 275-278.

Nicholson, G.E., 1990, Structural overview of Elk Hills, *in* J.G. Kuespert, and S.A. Reid, (eds.), Structure, stratigraphy, and hydrocarbon occurrences of the San Joaquin Basin, California: AAPG Pacific Section Guidebook, v. 64, p. 133–140.

Ratliff, R., 1992, Deformation studies of folding and faulting: cross section kinematics, strain analysis, and three-dimensional geometry: Ph.D. Dissertation, University of Colorado, Boulder, 510 p.

Reid, S.A., 1995, Miocene and Pliocene depositional systems of the southern San Joaquin basin and formation of sandstone reservoirs in the Elk Hills area, California, *in* A.E. Fritsche, (ed.), Cenozoic paleogeography of the western United States-II: Pacific Section SEPM, Book 75, p. 131–150.

Smalley, P.C., and A.H. Muggeridge, 2010, Reservoir compartmentalization: get it before it gets you: Geological Society London Special Publications, v. 347, p. 25-41.

Smith, D.A., 1980, Sealing and Nonsealing Faults in Louisiana Gulf Coast Salt Basin: AAPG Bulletin, v. 64, p. 145–172.

Townend, J., and M.D. Zoback, 2000, How faulting keeps the crust strong: Geology, v. 28, p. 399-402.

Van Hulten, F.F.N., 2010, Geological factors effecting compartmentalization of Rotliegend gas fields in the Netherlands: Geological Society London Special Publications, v. 347, p. 301-315.

Wiprut, D., and M.D. Zoback, 2002, Fault reactivation, leakage potential, and hydrocarbon column heights in the northern North Sea, *in* A.G. Koestler, and R. Hunsdale, (eds.), Hydrocarbon Seal Quantification: NPF Special Publication 11, p. 203–219.

Yielding, G., 2002, Shale Gouge Ratio - calibration by geohistory, *in* A.G. Koestler, and R. Hunsdale, (eds.), Hydrocarbon Seal Quantification: Norsk Petroleumsforening (NPF) Special Publication 11, p. 1–15.

Yielding, G., P. Bretan, and B. Freeman, 2010, Fault seal calibration: A brief review: Geological Society London Special Publications, v. 347, p. 243-255.

Yielding, G., B. Freeman, and D.T. Needham, 1997, Quantitative Fault Seal Prediction: AAPG Bulletin, v. 81, p. 897-917.

Zoback, M., C. Barton, T. Finkbeiner, and S. Dholakia, 1996, Evidence for Fluid Flow Along Critically Stressed Faults in Crystalline and Sedimentary Rock, *in* Faulting, Faults Sealing, and Fluid Flow in Hydrocarbon Reservoirs, G. Jones, Q. Fisher, and R. Knipe, (eds.), Leeds, England, University of Leeds, England. p. 47–48.

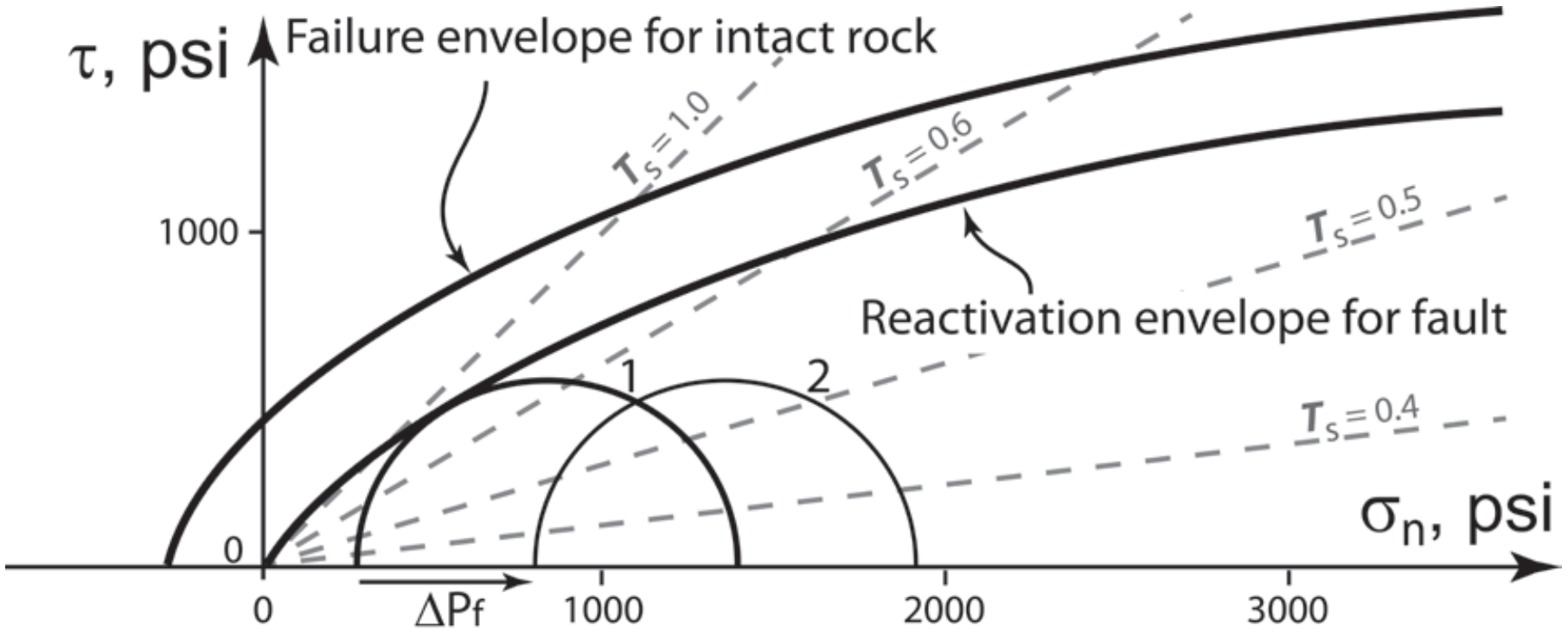


Figure 1. Mohr circle construction showing hypothetical failure envelope for intact rock, and the reactivation envelope for (cohesionless) faults. Mohr circle 1 represents the ambient stress state where *in situ* effective stress is balanced with respect to fault reactivation (Townend and Zoback, 2000). $\Delta P_f$ is the reduction in pore fluid pressure resulting from production, and Mohr circle 2 represents the changed stress state, now distant from the critical reactivation condition. Gray dashed lines are contours of slip tendency ($\boldsymbol{T}_S$). In crystalline rock, fractures with $\boldsymbol{T}_S \approx 0.6$ are hydraulically conductive (Townend and Zoback, 2000).

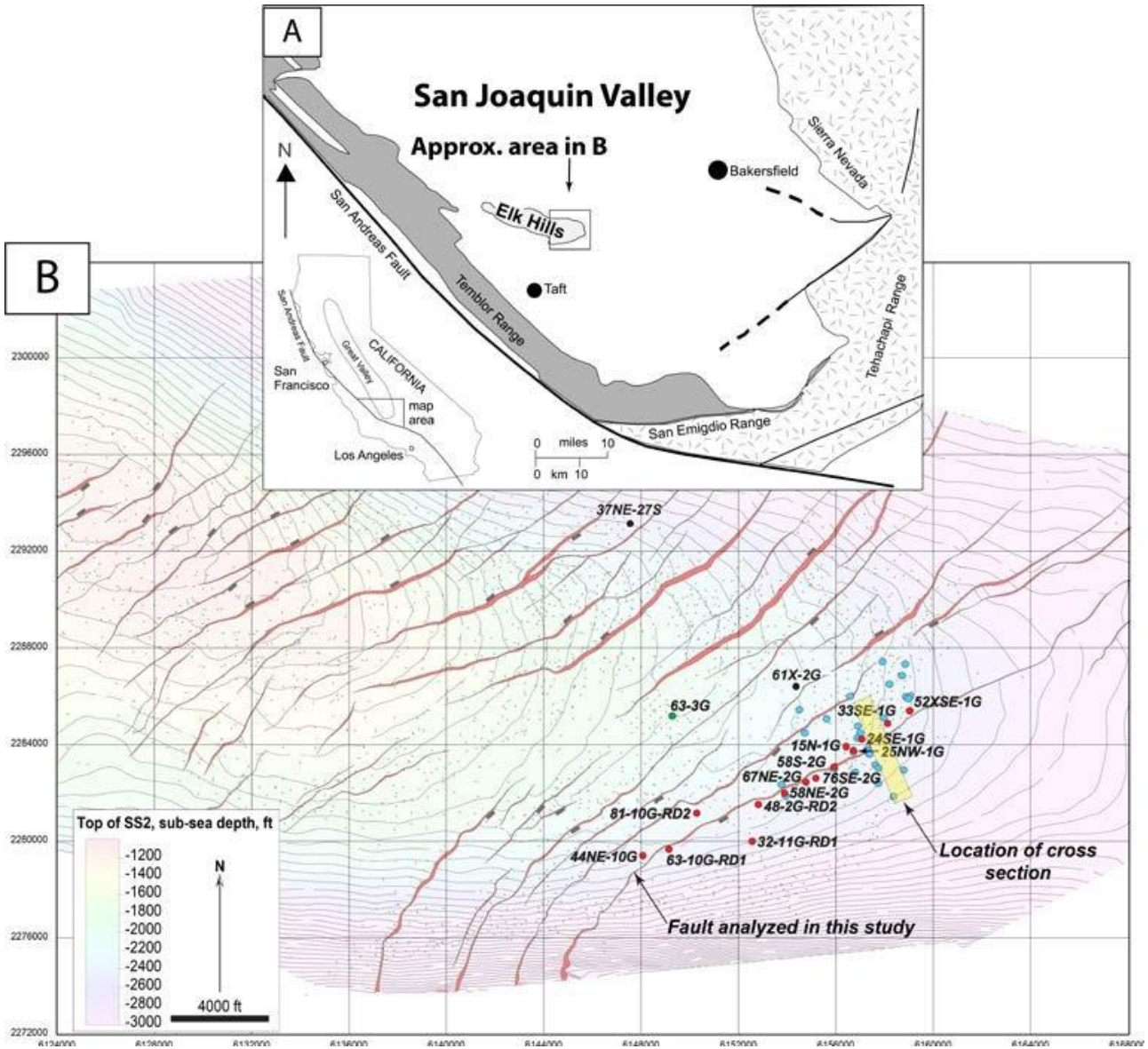


Figure 2. (A) Location map of Elk Hills after Reid (1995) showing the location of (B). (B) Map of depth of top of the Etchegoin Sub-Scalez 2 (SS2) horizon. Contours are in feet, grid is California state survey feet. Fault gaps in red. Rectangular marker on downthrown sides of major faults. Well locations mentioned in text (red – SGR, black – core, green – triaxial test data, blue – pressure data) and fault used in this study are shown together with the location of the schematic cross section in Figure 4B. Pressure data wells (blue) are not labeled.

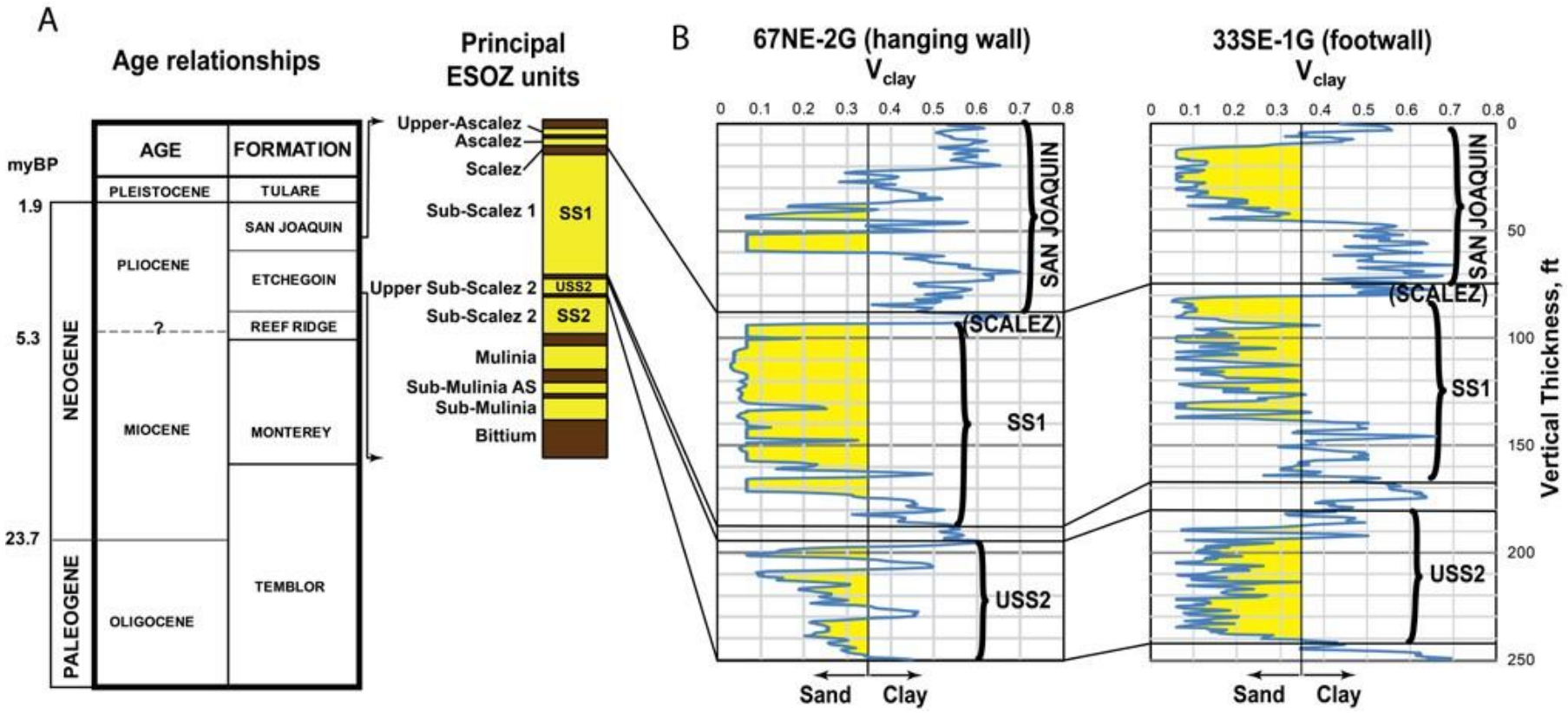


Figure 3. (A) Age relationships of the principal units within the ESOZ. (B) Example $V_{clay}$ logs of the units used in this analysis and the lowermost San Joaquin above, from wells 67NE-2G and 33SE-1G. Vertical scales are in feet. These two wells are on opposite sides of the fault and about 1 mile apart.

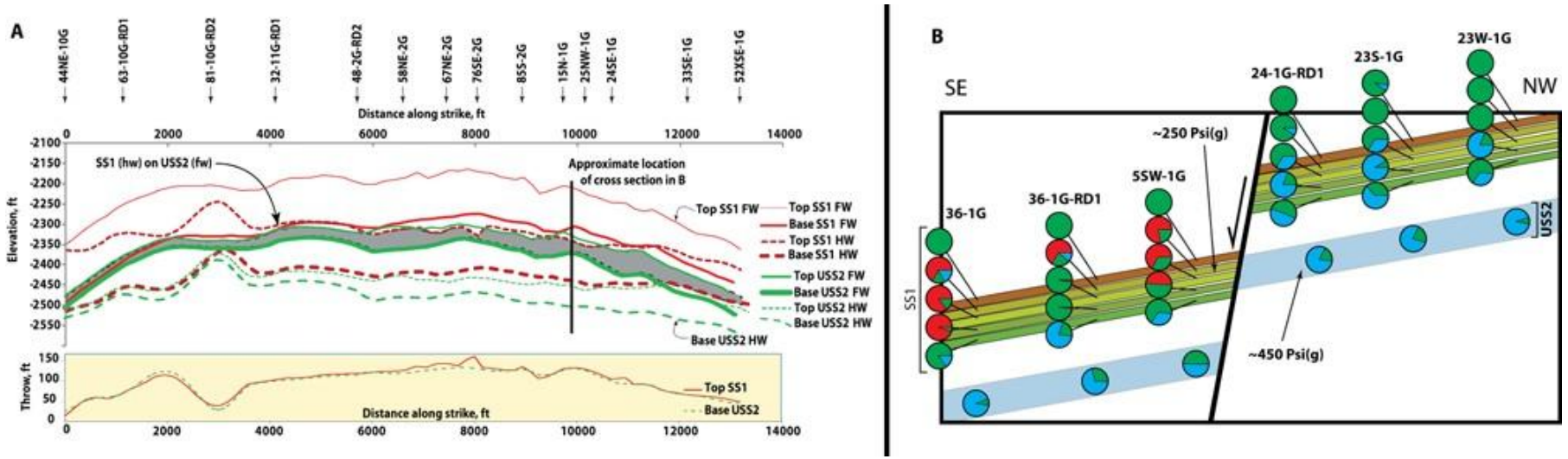


Figure 4. (A) Juxtaposition (Allan) diagram of part of fault FB11C-12SE. Projected locations of the fourteen wells used for analysis are shown along top. FW – footwall, HW – hanging wall. Lower graph are throw profiles for the two reservoirs analyzed for this section of the fault. Area shaded gray denotes juxtaposition of SS1 in the hanging wall and the USS2 in the footwall across the fault. (B) Schematic cross-section approximately 4000 ft (1219 m) long through fault FB11C-12SE (approximate throw = 140 ft [43 m]) near well 15N-1G to illustrate phase and pressure differentials using data from wells within a radius of 0.6 mile (1 km). The pie charts illustrate the proportion of fluids logged in the open hole for six wells along the line of section from the stratigraphic units as shown. In the pie charts, red is gas, green is oil, light blue is water.

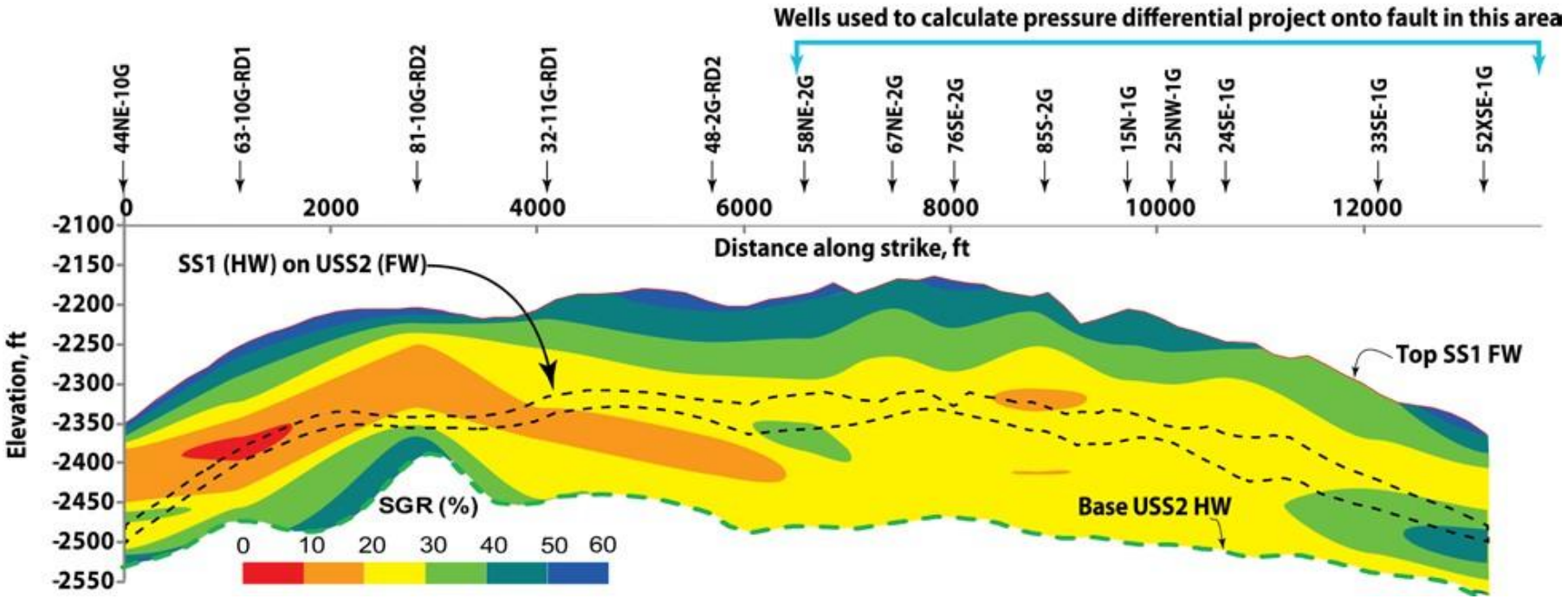


Figure 5. Same fault-perpendicular view of fault FB11C-12SE as in Figure 4A with SGR plotted. The projected locations of the fourteen wells used to calculate SGR are shown. The area onto which the wells used to calculate pressure differential project is indicated, see Figure 2B for locations of these wells. Area outlined in dashed black is the juxtaposition across the fault of SS1 in the hanging wall and USS2 in the footwall.

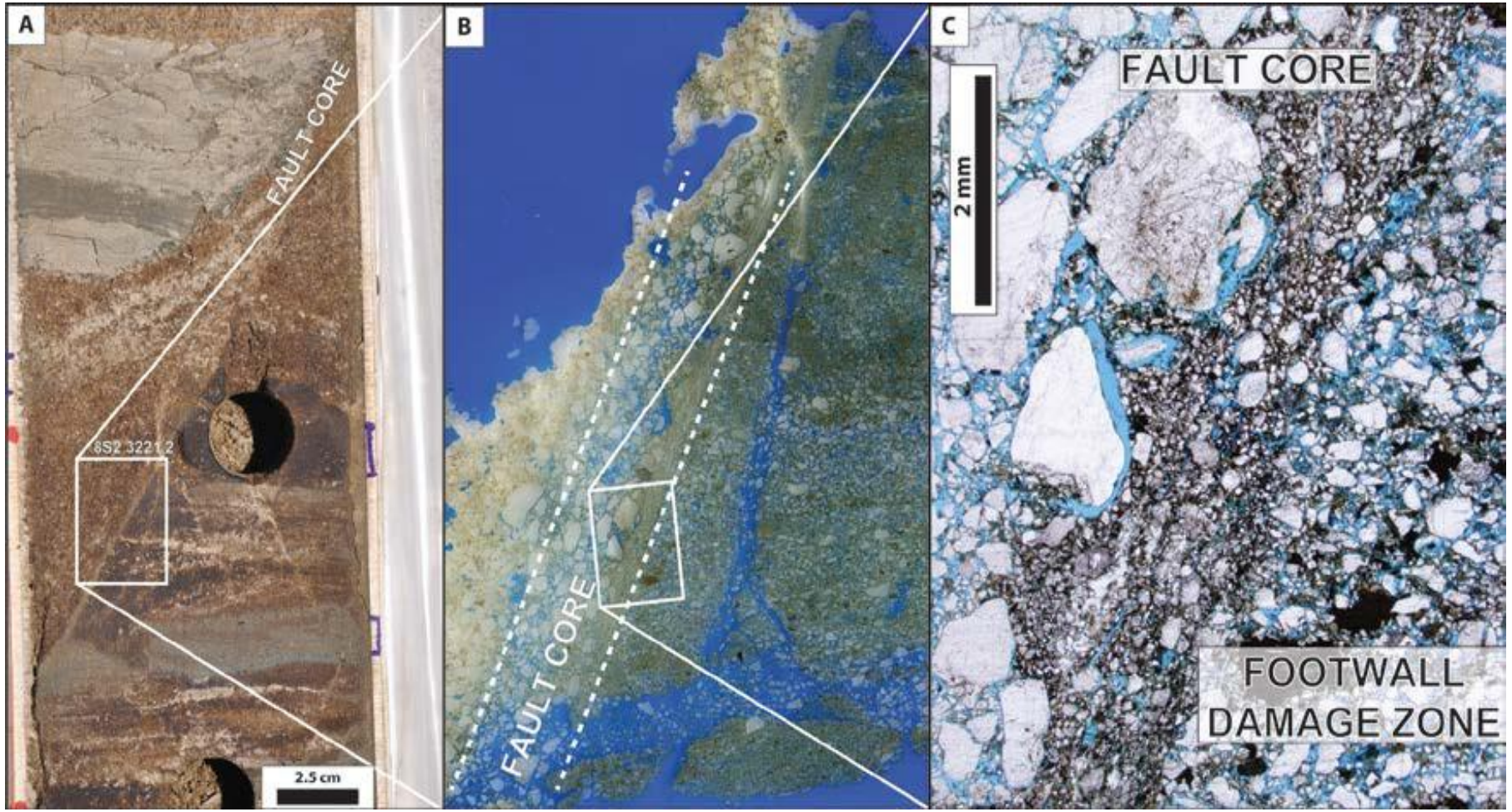


Figure 6. (A) Core photograph at drilled depth 3221.2 ft (982 m) from well 37NE-27S. A normal fault with displacement of approximately 2 ft (0.6 m) self-juxtaposes sand layer within SS1. Illumination is from the right, casting shadows into core-plug sample holes. (B) Full thin section of cross-fault area shown in (A). Thin section is mounted using blue epoxy. (C) Photomicrograph in plane polarized light of area indicated in (B). The fault zone shows evidence of grain size reduction and entrainment of fine grained material into the fault zone.

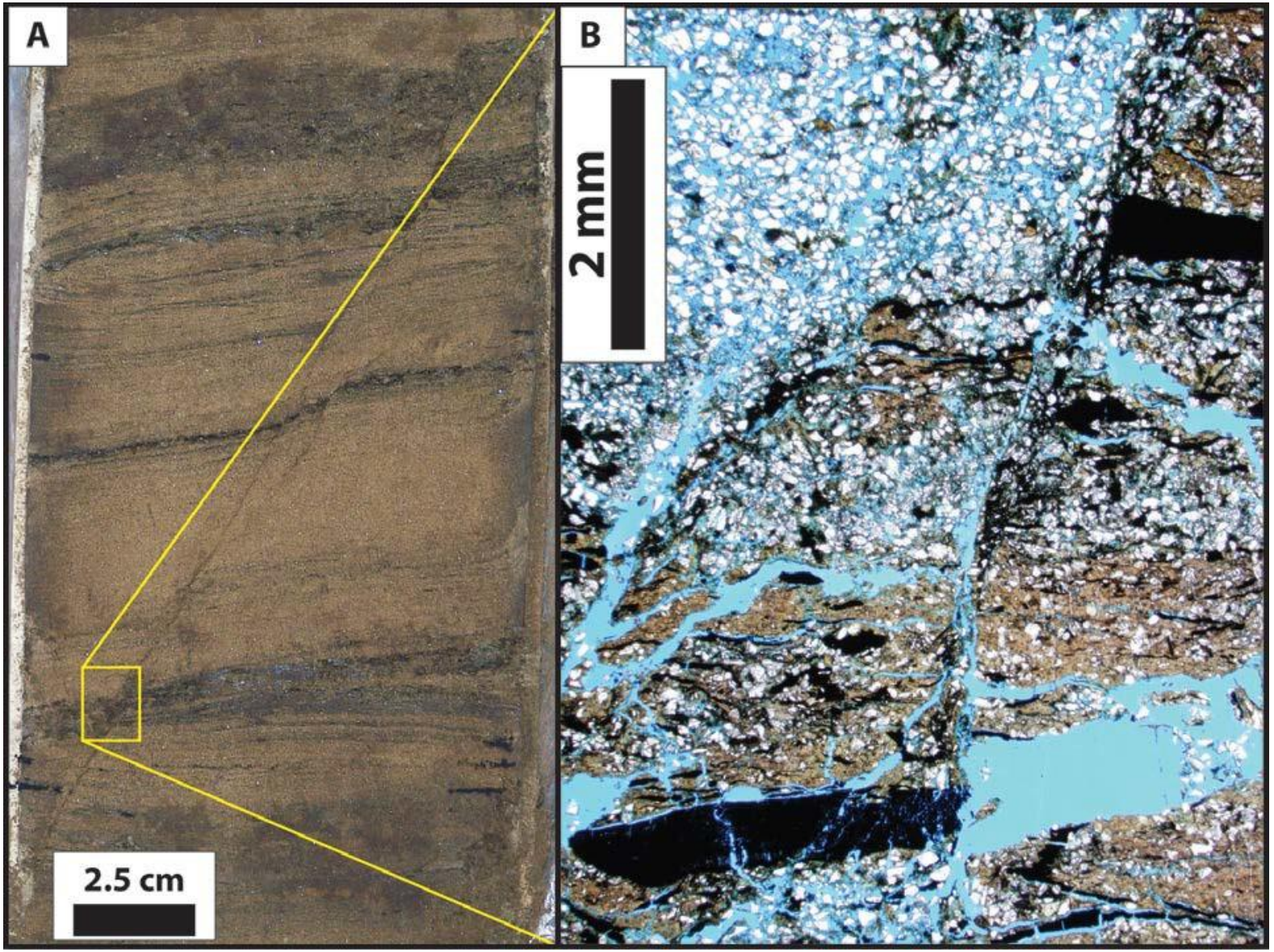


Figure 7. (A) Core photograph at drilled depth 2976.2 ft (907 m) from well 61X-2G. A normal fault with displacement of less than an inch (3 mm) self-juxtaposes sand layer within SS1. (B) Photomicrograph in plane polarized light of area indicated in (A). The fault zone shows evidence of entrainment and alignment of fine- grained material into the fault zone (shale gouge and/or smear). In addition, the fault is part of a zone of fault segments and synthetically dipping layers that all contribute to a reduction in cross-fault permeability.

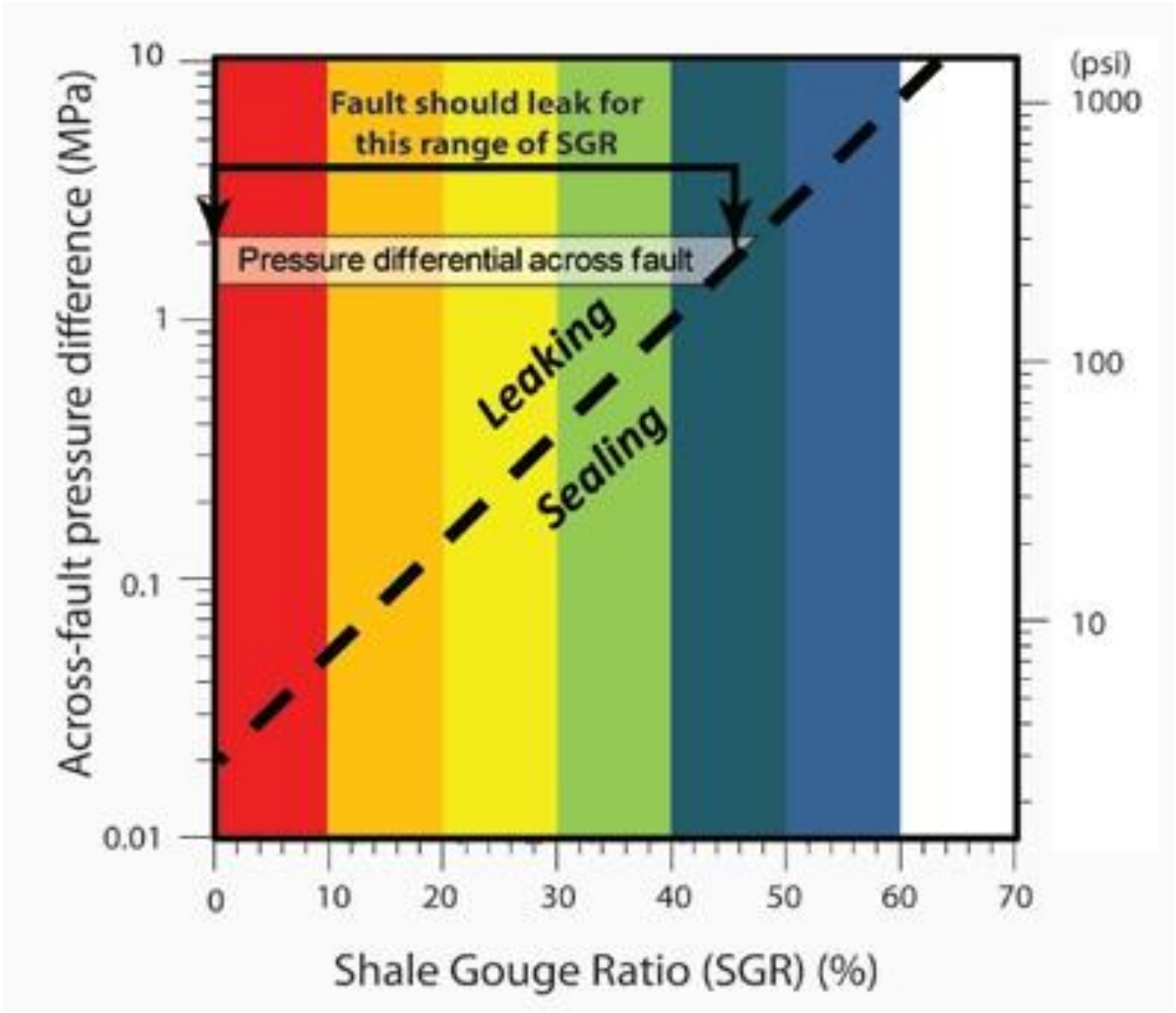


Figure 8. Long term, or static, pressure differences that can be supported by different shale gouge ratios (after Yielding, 2002). The dashed line represents the boundary between sealing and leaking behavior for rocks at less than 3000 m (9842 ft) depth. The fault studied in detail here has a large area of sand-on-sand juxtaposition with SGR values of 0 to 30 %; however, it supports a short term, dynamic, pressure differential of between 230 and 300 psi (1.6 to 2.1 MPa).

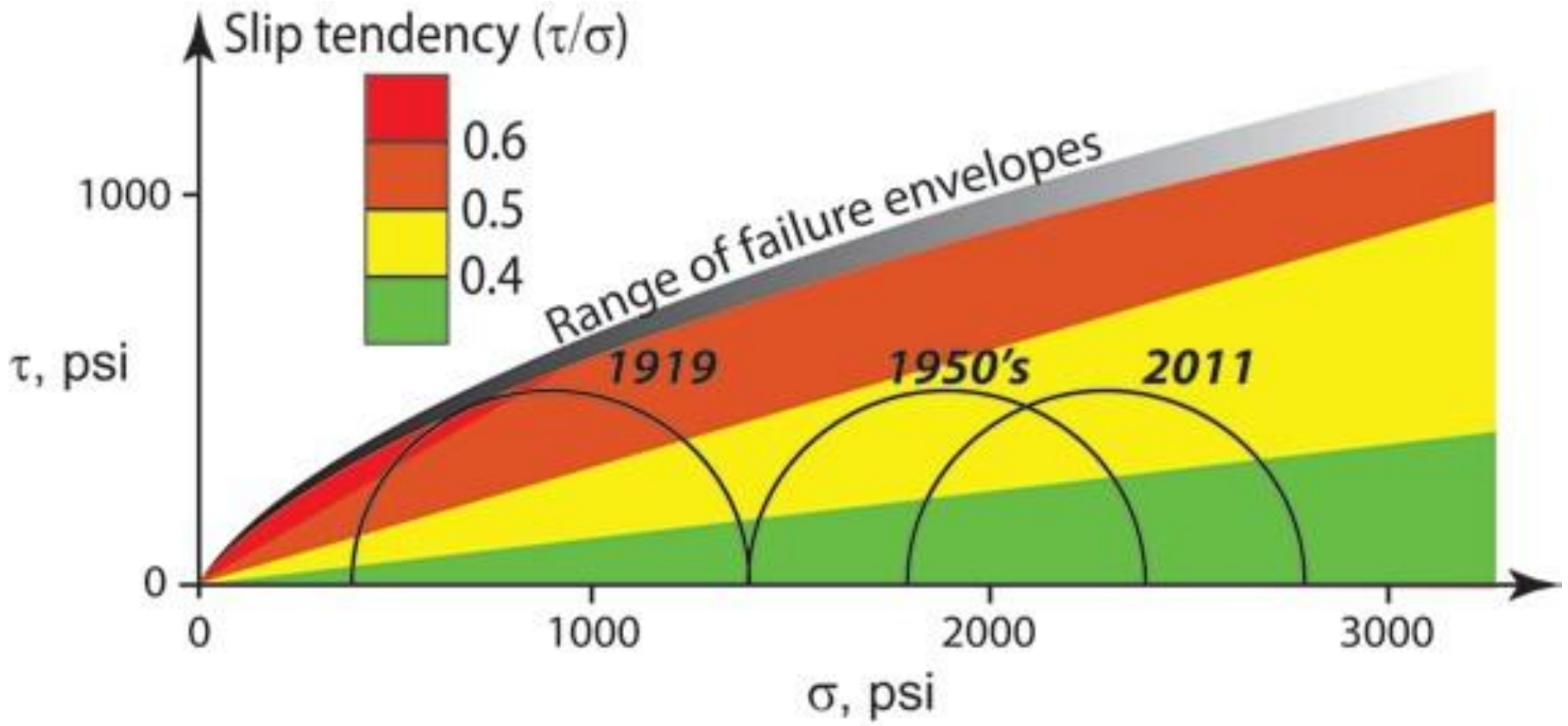


Figure 9. Mohr-circle plot of likely stress states in Elk Hills ESOZ. Gray shaded area represents range of failure envelopes based on triaxial test data. Mohr circles represent the evolving stress state from active faulting over the Elk Hills anticline prior to discovery, through the 1950's to the present-day. Background colors represent ranges of slip tendency (Morris et al., 1996) in Mohr circle space.